Microfluidics and Nanofluidics (2022) 26:64
https://doi.org/10.1007/s10404-022-02569-5

RESEARCH PAPER

Investigation of MHD effects on micropolar–Newtonian fluid flow through composite porous channel

Satya Deo[1] · **Deepak Kumar Maurya**[1,2]

Received: 28 March 2022 / Accepted: 3 July 2022 / Published online: 28 July 2022

Abstract

The present study investigates the influence of uniform magnetic field on the flow of a Newtonian fluid sandwiched between two micropolar fluid layers through a rectangular (horizontal) porous channel. Fluid flow in the every region is steady, incompressible and the fluids are immiscible. Uniform magnetic field is applied in a direction perpendicular to the direction of fluid motion. The governing equations of micropolar fluid are expressed in Eringen's approach and further modified by Nowacki's approach. For respective porous channels, expressions for linear velocity, microrotations, stresses (shear and couple) are obtained analytically. Continuity of velocities, continuity of microrotations and continuity of stresses are employed at the porous interfaces; conditions of no slip and no spin are applied at the impervious boundaries of the composite channel. Numerical values of flow rate, wall shear stresses and couple stresses at the porous interfaces are evaluated by MATHEMATICA and listed in tables. Graphs of flow rate and fluid velocity are plotted and their behaviors discussed.

Keywords Micropolar fluids · Newtonian fluid · Couple stress · Hartmann number · Flow rate

Mathematics Subject Classification 76A05 · 76S05 · 76W05 · 35C05

List of symbols

Non − dimensional symbols	Description
H	Hartmann number
M	Micropolar parameter
L	Couple stress parameter
Λ	Conductivity ratio parameter
ϕ	Viscosity ratio
Symbols	Description [S.I. Units]
h^*	Width of channel [meter]
U^*	Uniform fluid velocity [meter-second^{-1}]
p^*	Fluid pressure [Pascal]
u^*	Horizontal velocity [meter-second^{-1}]
w^*	Microrotation vector [second^{-1}]
v^*	Fluid velocity vector [meter-second^{-1}]
J^*	Electrical current density [Ampere-meter^{-2}]
B^*	Magnetic field [Tesla]
E^*	Electric field [Newton-Coulomb^{-1}]
σ^*	Electrical conductivity [Siemens-meter^{-1}]
k^*	Permeability [Meter^2]
T^*_{yx}	Tangential stress [second^{-1}]
m^*_{yz}	Couple stress [meter^{-1} second^{-1}]
∇^*	Gradient operator [meter^{-1}]
(μ^*_e, κ^*_e)	Viscosity coefficients in Eringen's approach [Poise]
(μ^*, κ^*)	Fluid viscosity coefficients [Poise]
$(\alpha^*_e, \beta^*_e, \gamma^*_e)$	Angular viscosity coefficients [Poise meter^2]

✉ Deepak Kumar Maurya
deepak893395@gmail.com

Satya Deo
satyadeo@allduniv.ac.in

1 Department of Mathematics, University of Allahabad, Prayagraj 211002, UP, India

2 Department of Mathematics, Prof. Rajendra Singh (Rajju Bhaiya) Institute of Physical Sciences for Study and Research, V.B.S. Purvanchal University, Jaunpur 222003, UP, India

$(\alpha^*, \delta^*, \tau^*)$	Gyro-viscosity coefficients [Poise meter^2]
(x^*, y^*, z^*)	Cartesian coordinates [meter]

1 Introduction

Micropolar fluids respond to micro-rotational motions and spin inertia which can support stress moments (*i.e. couple stresses*) and body moments (*i.e. body couples*) (Lukaszewicz 1999). Motion of micropolar fluids can represent the various effects that are not possible in non-polar Stokesian fluids, given in the book by Stokes (1984). Eringen (1966) reported the fundamental concepts on micropolar fluids consisting of the effects of couple stresses and microstructure. An explicit dependence on components of deformation tensors was reported by Nowacki (1970). In the presence of magnetic field, an incompressible and electrically conducting micropolar fluid flow through a rectangular channel with suction and injection was reported by Murthy et al. (2011). Srinivasacharya et al. (2001) observed the unsteady incompressible micropolar fluid motion between two porous plates with a periodic injection/suction. Yadav et al. (2018) formulated a mathematical model for the flow of two immiscible fluids through a porous horizontal channel and obtained its analytical solution using direct method. Yadav et al. (2018) reported steady and incompressible fluid flow of an Eringen fluid sandwiched between two Newtonian fluid layers flowing through a porous channel. Perturbation solutions were obtained for a diverging channel filled with conducting micropolar fluid by Srinivasacharya and Shiferaw (2009). Jaiswal and Yadav (2020) investigated the effect of width of the layers on the micropolar–Newtonian fluid flow through the porous layered rectangular channel by sandwiching of non-Newtonian fluid between the Newtonian fluid layers. Sherief et al. (2014) reported the quasi-steady micropolar fluid flow between two coaxial cylinders by considering two types of flow problems: one is flow parallel to axes of cylinders and other is the flow perpendicular to axes of cylinders. Lok et al. (2018) reported flow of a micropolar fluid over a extensible surface on applying the slip condition. Deo et al. (2020) investigated the Stokesian flow of a micropolar fluid through a cylindrical tube enclosing an impermeable core coated with porous layer in the presence of external magnetic field. Deo et al. (2021) reported the magnetic effects on hydrodynamic permeability of biporous membrane relative to the flow of micropolar liquid using four known cell models. In addition, Maurya et al. (2021) investigated the Stokes flow of non-Newtonian fluid flow through a porous cylinder and compared the flow patterns for two types of BVPs.

Krishna et al. (2019) considered the unsteady magnetohydrodynamic convection flow of an incompressible, viscous and heat-absorbing fluid over a flat plate. Asia et al. (2016) investigated the flow and heat transfer characteristics of an electrically conducting micropolar fluid using different methods. Krishna et al. (2020) studied the effects of Hall and ion slip on MHD rotating flow of ciliary propulsion and mixed convective flow past an infinite porous plate. Krishna et al. (2019) studied the Soret and Joule effects of magnetohydrodynamic flow of an incompressible and electrically conducting viscous fluid past an infinite vertical porous plate. Krishna and Chamkha (2022) investigated the hall and ion slip effects on the flow of micropolar and elasticoviscous fluid between two porous surfaces.

Porosity of a porous medium is fraction of the total volume of medium that is occupied by void space (Nield and Bejan 2006). Brinkman (1947) improved the Darcy's law for porous medium with an appropriate combination of the usual Darcy term analogous to the Laplacian terms. Deo and Maurya (2019) obtained the generalized stream function solution of the Brinkman equation in the cylindrical polar coordinates. Recently, Maurya and Deo (2020) reported the analytical solution of Brinkman and Stokes equations in the parabolic cylindrical coordinates. On using cell model techniques, hydrodynamic permeability of biporous medium composed by porous cylindrical particles which is located in another porous medium was investigated by Yadav et al. (2013). In the porous channel, fully developed flow of an incompressible, electrically conducting viscous fluid through a porous medium of variable permeability in the presence of transverse magnetic field was studied in Srivastava and Deo (2013). Umavathi et al. (2010) reported the analytical concept of Couette flow and heat transfer in a composite channel. Recently, Maurya and Deo (2022) investigated the MHD effects on micropolar–Newtonian fluid flows through coaxial cylindrical shells.

In this research work, the magnetohydrodynamic effects on Newtonian fluid flowing through a porous channel, sandwiched between two rectangular porous channels filled with micropolar fluids have been investigated. The direction of fluid flow is taken along x^*-axis and the uniform magnetic field is applied in a direction perpendicular to the direction of fluid flow. For the corresponding fluid flow regions, velocity profiles, shear stresses, couple stresses and flow rate are obtained. Numerical values of the shear wall stresses and couple wall stresses at the porous interfaces are also tabulated. The volumetric flow rate and fluid velocity are plotted and discussed for different values of flow parameters.

2 Flow assumptions

- Fluid is flowing through the porous channels with constant pressure gradient.
- It is supposed that both outer boundaries of the composite channel are impervious and fluids are electrically conducting.
- Assume that induced magnetic field is very small in the comparison of the external magnetic field ($\mathbf{B}^*$).
- Fluids are immiscible and flow in each porous channel is steady, laminar and fully developed.
- The applied fluid pressure p^* is same for both the micropolar and Newtonian fluids.
- Assume that the magnetic Reynolds number is very small and external electric field ($\mathbf{E}^*$) is absent so that the induced electric current can be neglected.

3 Mathematical formulation

The mathematical model of the present investigation is based on the sandwiching of Newtonian fluid between two non-Newtonian fluid layers through a horizontal porous channel. The horizontal composite porous channel is divided into three porous layers of equal width h^*. The external magnetic field is of uniform strength, applied in a direction perpendicular to the flow. Here, modified Brinkman's model for momentum equation is used to investigate the Newtonian fluid, and the governing equations for micropolar fluid proposed by Nowacki, are applied.

Assuming that the electrically conducting immiscible fluids are flowing with characteristic velocity U^* along the x^* -axis in the presence of uniform magnetic field B^*. The lower porous channel ($0 \le y^* \le h^*$) and the upper porous channel ($2h^* \le y^* \le 3h^*$) are filled with micropolar fluids having permeability ${k_1}^*$ and ${k_3}^*$, respectively. The sandwiched porous channel *i.e.* middle channel ($h^* \le y^* \le 2h^*$) is filled with Newtonian fluid having permeability ${k_2}^*$ (Fig. 1).

In the Eringen approach (Eringen 1966), governing equations of an incompressible steady micropolar fluid flow, in the absence of magnetic field, body forces and body couples, are given by

$$\nabla^* \cdot \mathbf{v}^* = 0, \tag{3.1}$$

$$\left(\frac{\mu_e^* + \kappa_e^*}{k^*}\right)\mathbf{v}^* + \nabla^* p^* - \frac{\kappa_e^*}{2}\nabla^* \times \mathbf{w}^* + (\mu_e^* + \kappa_e^*)\,\nabla^* \times \nabla^* \times \mathbf{v}^* = \mathbf{0}, \tag{3.2}$$

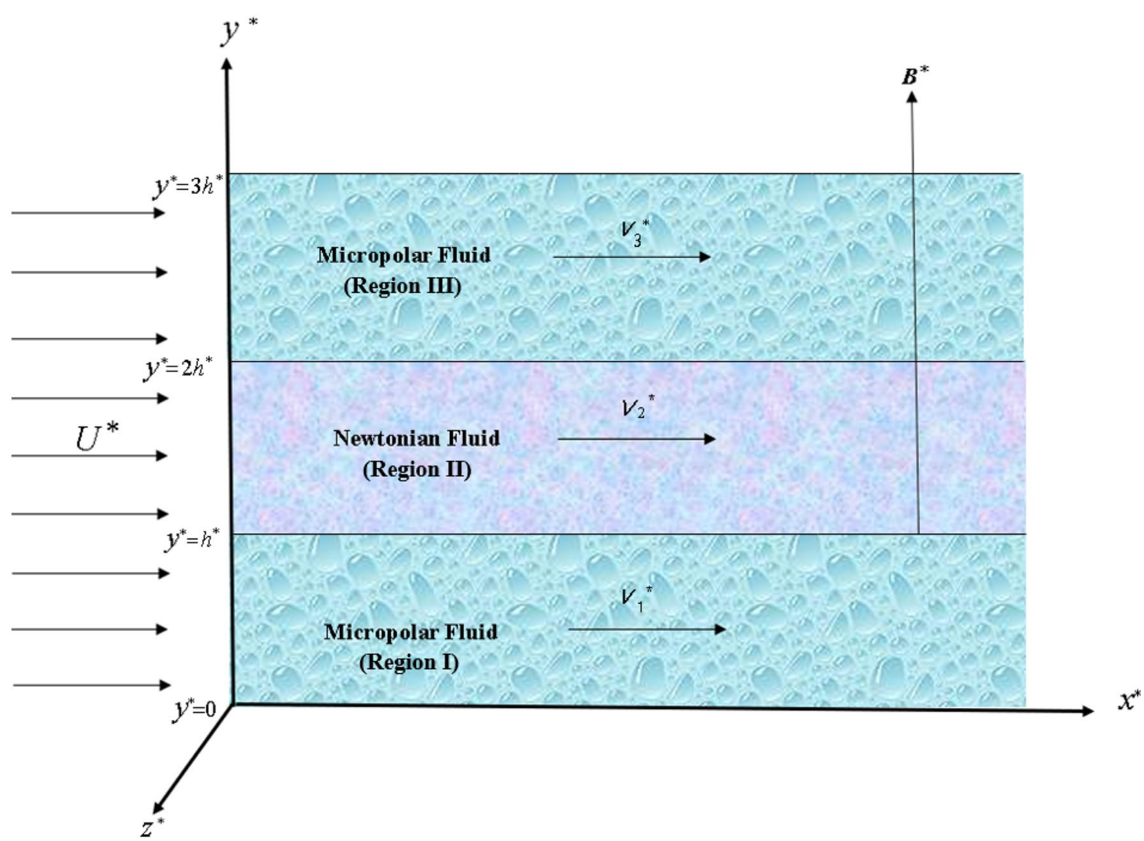

Fig. 1 Geometry of the problem

$$
\begin{aligned}
&-2\kappa_e^*\mathbf{w}^* + \kappa_e^*\nabla^*\times\mathbf{v}^* - \gamma_e^*\nabla^*\times\nabla^*\times\mathbf{w}^* \\
&\quad + (\alpha_e^* + \beta_e^*)\nabla^*(\nabla^*\cdot\ \mathbf{w}^*) = \mathbf{0},
\end{aligned}
\tag{3.3}
$$

where k^* is the permeability of the porous medium, $\mathbf{v}^*$, $\mathbf{w}^*$ and p^* are representing the fluid velocity vector, microrotation vector and fluid pressure at any point of the fluid region, respectively. The material's constants (μ_e^*, κ_e^*) are viscosity coefficients and $(\alpha_e^*, \beta_e^*, \gamma_e^*)$ are angular-viscosity coefficients of the micropolar fluid.

Stokes (1984) suggested to redefine viscosity coefficients using simple replacement $\mu_e^* = \mu^* - \kappa^*$ and $\kappa_e^* = 2\kappa^*$. Nowacki (1970) proposed to choose angular-viscosity coefficients as $\gamma_e^* = \delta^* + \tau^*$, $\beta_e^* = \delta^* - \tau^*$ and $\alpha_e^* = \alpha^*$. In the presence of uniform magnetic field B^*, governing equations (Yadav et al. 2018) of an incompressible steady micropolar fluid flow through the porous channels $(0 \le y^* \le h^*)$ and $(2h^* \le y^* \le 3h^*)$, in the absence of body forces and body couples, are given by

$$
\nabla^*.\mathbf{v}_i^* = 0,
\tag{3.4}
$$

$$
\begin{aligned}
&\left(\frac{\mu^* + \kappa^*}{k_i^*}\right)\mathbf{v}_i^* + \nabla^* p^* - \kappa^*\nabla^*\times\mathbf{w}_i^* \\
&\quad + (\mu^* + \kappa^*)\nabla^*\times\nabla^*\times\mathbf{v}_i^* - \mathbf{J}_i^*\times\mathbf{B}^* = \mathbf{0},
\end{aligned}
\tag{3.5}
$$

$$
\begin{aligned}
&-2\kappa^*\mathbf{w}_i^* + \kappa^*\nabla^*\times\mathbf{v}_i^* - (\delta^* + \tau^*)\nabla^*\times\nabla^*\times\mathbf{w}_i^* + (\alpha^* \\
&\quad + \delta^* - \tau^*)\nabla^*(\nabla^*\cdot\ \mathbf{w}_i^*) = \mathbf{0},
\end{aligned}
\tag{3.6}
$$

where $\mathbf{v}_i^*$, $\mathbf{w}_i^*$ are representing the velocity vectors and microrotation vectors of micropolar fluid for lower porous channel $(i = 1)$ and upper porous channel $(i = 3)$, at any point (x^*, y^*, z^*), respectively.

The governing equations (Brinkman 1947) for Newtonian fluid through the porous channel $(h^* \le y^* \le 2h^*)$, in the presence of uniform magnetic field and in the absence of body forces, are given by

$$
\nabla^*\cdot\mathbf{v}_2^* = 0\,,
\tag{3.7}
$$

$$
-\nabla^* p^* - \frac{{\mu_2}^*}{{k_2}^*}\,\mathbf{v}_2^* - {\mu_2}^*\,\nabla^*\times\nabla^*\times\mathbf{v}_2^* + \mathbf{J}_2^*\times\mathbf{B}^* = \mathbf{0},
\tag{3.8}
$$

where velocity and dynamic viscosity of the Newtonian fluid are represented by $\mathbf{v}_2^*$ and μ_2^*, respectively. The material's constants (μ^*, κ^*) are viscosity coefficients and $(\alpha^*, \delta^*, \tau^*)$ are gyro-viscosity coefficients. These viscosity coefficients are related by inequalities:

$$
\begin{aligned}
&\mu^* \ge 0,\ \kappa^* \ge 0,\ \delta^* \ge 0,\ \delta^* + \tau^* \ge 0,\ 3\alpha^* + 2\delta^* \ge 0, \\
&\quad -(\delta^* + \tau^*) \le (\delta^* - \tau^*) \le (\delta^* + \tau^*).
\end{aligned}
$$

By Ohm's law, $\mathbf{J}_i^* = \sigma_i^*(\mathbf{E}^* + \mathbf{v}_i^*\times\mathbf{B}^*)$, where $\sigma_i^*(i = 1, 2, 3)$ and $\mathbf{E}^*$ stand for electrical conductivity of micropolar fluid and electric field, respectively. Therefore,

$$
\mathbf{J}_i^*\times\mathbf{B}^* = -\sigma_i^* B^{*2}\,\mathbf{v}_i^*,
\tag{3.9}
$$

where $B^* = |\mathbf{B}^*|$. To treat governing equations of the micropolar fluid flow problem into dimensionless form, some non-dimensionalizing variables are introduced:

$$
\begin{aligned}
&\mathbf{v}_i = \frac{\mathbf{v}_i^*}{U^*}, \mathbf{w}_i = \frac{h^*\mathbf{w}_i^*}{U^*}, \\
&y = \frac{y^*}{h^*}, p = \frac{h^* p^*}{\mu^* U^*}, {\eta_i}^2 = \frac{h^{*2}}{{k_i}^*}, \\
&\Lambda_1 = \frac{\sigma_2^*}{\sigma_1^*}, \Lambda_3 = \frac{\sigma_2^*}{\sigma_3^*}, \\
&\phi = \frac{\mu_2^*}{\mu^*}, H = B^* h^*\sqrt{\frac{\sigma_2^*}{\mu^*}}, H_1 = \frac{H}{\sqrt{\Lambda_1}}, H_3 = \frac{H}{\sqrt{\Lambda_3}}, \\
&M^2 = \frac{\kappa^*}{\mu^* + \kappa^*}, \\
&L^2 = \frac{\delta^* + \tau^*}{2\mu^* h^{*2}}, W^2 = \frac{\alpha^* + \delta^* - \tau^*}{2\mu^* h^{*2}}.
\end{aligned}
$$

Here, H is the Hartmann number $(0 \le H < \infty)$, M is micropolar parameter $(0 \le M < 1)$ and L is couple stress parameter $(0 \le L < \infty)$. The non-dimensional form of the governing equations (3.4)–(3.6) for $i = 1, 3$, are

$$
\nabla\cdot\mathbf{v}_i = 0,
\tag{3.10}
$$

$$
\begin{aligned}
&\nabla p + \left(\frac{{\eta_i}^2}{1 - M^2} + {H_i}^2\right)\mathbf{v}_i - \frac{M^2}{1 - M^2}\,\nabla\times\mathbf{w}_i \\
&\quad + \frac{1}{1 - M^2}\,\nabla\times\nabla\times\mathbf{v}_i = \mathbf{0},
\end{aligned}
\tag{3.11}
$$

$$
\begin{aligned}
&\mathbf{w}_i - \frac{1}{2}\,\nabla\times\mathbf{v}_i + \frac{L^2(1 - M^2)}{M^2}\,\nabla\times\nabla \\
&\quad \times\mathbf{w}_i - \frac{W^2(1 - M^2)}{M^2}\,\nabla(\nabla\cdot\mathbf{w}_i) = \mathbf{0}.
\end{aligned}
\tag{3.12}
$$

Similarly, the field equations (3.7) and (3.8) for middle channel are

$$
\nabla.\mathbf{v}_2 = 0,
\tag{3.13}
$$

$$
\nabla p = -\phi\,\eta_2^2\,\mathbf{v}_2 + \phi\,\nabla^2\mathbf{v}_2 - H^2\,\mathbf{v}_2.
\tag{3.14}
$$

For micropolar fluid, the non-dimensional form of tangential stresses $(T_{yx(i)})$ and couple stresses $(m_{yz(i)})$ for $i = 1, 3$ are

$$T_{yx(i)} = \left[\frac{1}{1-M^2}\left(\frac{du_i}{dy}\right) + \left(\frac{M^2}{1-M^2}\right) w_i\right]$$
$$\text{and } m_{yz(i)} = \left[\frac{dw_i}{dy}\right]. \tag{3.15}$$

For Newtonian fluid, the non-dimensional form of tangential stress ($T_{yx(2)}$) will be

$$T_{yx(2)} = \phi \frac{du_2}{dy}. \tag{3.16}$$

4 Analytical solution

4.1 For lower and upper channels

The fluid velocities $\mathbf{v}_i$ and microrotation vectors $\mathbf{w}_i$ for plane Poiseuille flow of micropolar fluid along the x-axis of lower ($i = 1$) and upper ($i = 3$) porous channels are $\mathbf{v}_i = (u_i(y),\ 0,\ 0)$ and $\mathbf{w}_i = (0,\ 0, w_i(y))$, respectively. Therefore, governing equations (3.10)–(3.12) will assume the form

$$(D^2 - s_i^2)(D^2 - \varepsilon_i^2)u_i = -\frac{PM^2}{L^2}, \tag{4.1}$$

where

$$s_i^2 + \varepsilon_i^2 = \frac{(-2+M^2)M^2}{2L^2(-1+M^2)} + \eta_i^2 - (-1+M^2){H_1}^2,$$
$$s_i^2\varepsilon_i^2 = \frac{M^2}{L^2(-1+M^2)}[(-1+M^2){H_1}^2 - \eta_i^2],$$

and pressure gradient $P = \frac{dp}{dx}$ is taken constant.

The general solution of Eq. (4.1) represents velocity of the micropolar fluid and it comes out as

$$u_i(y) = A_i\, e^{s_i y} + B_i\, e^{-s_i y} + C_i\, e^{\varepsilon_i y} + D_i e^{-\varepsilon_i y} - \frac{PM^2}{s_i^2\varepsilon_i^2 L^2}, \tag{4.2}$$

where A_i, B_i, C_i, and D_i ($i = 1, 3$) are arbitrary parameters.

The microrotation component can be computed using following expression:

$$w_i = \left(-\frac{1}{2} + \frac{L^2(1-M^2)}{M^4}\left(\eta_i^2 + (1-M^2){H_i}^2\right)\right) \frac{du_i}{dy} - \frac{L^2(1-M^2)}{M^4}\frac{d^3u_i}{dy^3}. \tag{4.3}$$

Therefore, we have

$$w_i = \left(\frac{L^2\left(M^2-1\right)\left(H_i^2\left(M^2-1\right)-\eta_i^2\right)}{M^4} - \frac{1}{2}\right) \left(A_i s_i e^{s_i y} - B_i s_i e^{-s_i y} + \epsilon_i e^{-y\epsilon_i}\left(C_i e^{2y\epsilon_i} - D_i\right)\right) - \frac{L^2\left(1-M^2\right)}{M^4}\left(A_i s_i^3 e^{s_i y} - B_i s_i^3 e^{-s_i y} + \epsilon_i^3 e^{-y\epsilon_i}\left(C_i e^{2y\epsilon_i} - D_i\right)\right). \tag{4.4}$$

The tangential stresses for corresponding micropolar fluid regions are

$$T_{yx(i)} = \frac{1}{2M^2\left(1-M^2\right)} \Big[A_i s_i e^{s_i y}\left(2L^2\left(M^2-1\right)\left(-\eta_i^2 + H_i^2\left(M^2-1\right) + s_i^2\right) - M^2\left(M^2-2\right)\right) + e^{-y\left(s_i+\epsilon_i\right)}\left(\epsilon_i e^{s_i y}\left(C_i e^{2y\epsilon_i} - D_i\right)\left(2L^2\left(M^2-1\right)\left(-\eta_i^2 + H_i^2\left(M^2-1\right) + \epsilon_i^2\right) - M^2\left(M^2-2\right)\right) - B_i s_i e^{y\epsilon_i}\left(2L^2\left(M^2-1\right)\left(-\eta_i^2 + H_i^2\left(M^2-1\right) + s_i^2\right) - M^2\left(M^2-2\right)\right)\right)\Big]. \tag{4.5}$$

Couple stresses for corresponding micropolar fluid regions are

$$m_{yz(i)} = \left(\frac{L^2\left(M^2-1\right)\left(H_i^2\left(M^2-1\right)-\eta_i^2\right)}{M^4} - \frac{1}{2}\right) \left(A_i s_i^2 e^{s_i y} + B_i s_i^2 e^{-s_i y} + \epsilon_i^2 e^{-y\epsilon_i}\left(C_i e^{2y\epsilon_i} + D_i\right)\right) + \frac{L^2\left(M^2-1\right)}{M^4}\left[e^{-y\left(s_i+\epsilon_i\right)}\left(A_i s_i^4 e^{y\left(2s_i+\epsilon_i\right)} + B_i s_i^4 e^{y\epsilon_i} + \epsilon_i^4 e^{s_i y}\left(C_i e^{2y\epsilon_i} + D_i\right)\right)\right]. \tag{4.6}$$

4.2 For middle channel

The fluid velocity $\mathbf{v}_2$ for plane Poiseuille flow along the x-axis of the middle porous channel filled by Newtonian fluid is $\mathbf{v}_2 = (u_2(y),\ 0,\ 0)$. Therefore, Eqs. (3.13) and (3.14) will reduce to

$$\frac{d^2u_2}{dy^2} - \lambda^2 u_2 = \frac{P}{\phi}, \tag{4.7}$$

where $\lambda^2 = \eta_2^2 + \left(\frac{H^2}{\phi}\right)$.

Therefore, the analytical form of velocity vector of Newtonian fluid will be

$$u_2(y) = A_2\, e^{\lambda y} + B_2\, e^{-\lambda y} - \frac{P}{\lambda^2\phi}, \tag{4.8}$$

where A_2 and B_2 are arbitrary parameters.

Tangential stress for Newtonian fluid is

$$T_{yx(2)} = \lambda\phi e^{-\lambda y}\left(A_2\, e^{2\lambda y} - B_2\right). \tag{4.9}$$

5 Determination of arbitrary parameters

To determine ten parameters $A_1, B_1, C_1, D_1, A_2, B_2, A_3, B_3, C_3, D_3$, we will apply the following boundary conditions (Yadav et al. 2018) that are physically realistic and mathematically valid:

(i) no slip condition at $y = 0$ implies that

$$u_1 = 0. \tag{5.1}$$

(ii) no spin condition at $y = 0$ implies that

$$w_1 = 0. \tag{5.2}$$

(iii) continuity of the velocity at $y = 1$ implies that

$$u_1 = u_2. \tag{5.3}$$

(iv) continuity of tangential stress at $y = 1$ implies that

$$T_{yx(1)} = T_{yx(2)}. \tag{5.4}$$

(v) no couple stress at $y = 1$ implies that

$$m_{yz(1)} = 0. \tag{5.5}$$

(vi) continuity of the velocity at $y = 2$ implies that

$$u_2 = u_3. \tag{5.6}$$

(vii) continuity of tangential stress at $y = 2$ implies that

$$T_{yx(2)} = T_{yx(3)}. \tag{5.7}$$

(viii) no couple stress at $y = 2$ implies that

$$m_{yz(3)} = 0. \tag{5.8}$$

(ix) no slip condition at $y = 3$ implies that

$$u_3 = 0. \tag{5.9}$$

(x) no spin condition at $y = 3$ implies that

$$w_3 = 0. \tag{5.10}$$

Substituting the boundary conditions (BCs) from Eqs. (5.1) to (5.10), we will obtain a system of linear equations for the arbitrary parameters appearing in the solution of the velocities $u_1,\ u_2,\ u_3$. The system of linear equations can be expressed in matrix form in the following way:

$$NX = Z, \tag{5.11}$$

where matrices N, X and Z are

$$N = \begin{bmatrix} 1 & \xi_1 & e^{s_1} & -e^{s_1}\xi_2 & s_1 e^{s_1}\xi_1 & 0 & 0 & 0 & 0 & 0 \\ 1 & -\xi_1 & e^{-s_1} & e^{-s_1}\xi_2 & s_1 e^{-s_1}\xi_1 & 0 & 0 & 0 & 0 & 0 \\ 1 & \zeta_1 & e^{\varepsilon_1} & -e^{\varepsilon_1}\zeta_2 & \varepsilon_1 e^{\varepsilon_1}\zeta_1 & 0 & 0 & 0 & 0 & 0 \\ 1 & -\zeta_1 & e^{-\varepsilon_1} & e^{-\varepsilon_1}\zeta_2 & \varepsilon_1 e^{-\varepsilon_1}\zeta_1 & 0 & 0 & 0 & 0 & 0 \\ 0 & 0 & -e^{\lambda} & 0 & 0 & e^{2\lambda} & -e^{2\lambda}\Omega & 0 & 0 & 0 \\ 0 & 0 & -e^{-\lambda} & 0 & 0 & e^{-2\lambda} & e^{2\lambda}\Omega & 0 & 0 & 0 \\ 0 & 0 & 0 & 0 & 0 & -e^{2s_3} & -e^{2s_3}\xi_4 & s_3 e^{2s_3}\xi_3 & e^{3s_3} & e^{3s_3} \\ 0 & 0 & 0 & 0 & 0 & -e^{-2s_3} & e^{-2s_3}\xi_4 & s_3 e^{-2s_3}\xi_3 & e^{-3s_3} & -e^{-3s_3}\xi_3 \\ 0 & 0 & 0 & -e^{\lambda}\Omega & 0 & -e^{2\varepsilon_3} & -e^{2\varepsilon_3}\zeta_4 & \varepsilon_3 e^{2\varepsilon_3}\zeta_3 & e^{3\varepsilon_3} & e^{3\varepsilon_3}\zeta_3 \\ 0 & 0 & 0 & e^{-\lambda}\Omega & 0 & -e^{-2\varepsilon_3} & e^{-2\varepsilon_3}\zeta_4 & \varepsilon_3 e^{-2\varepsilon_3}\zeta_3 & e^{-3\varepsilon_3} & -e^{-3\varepsilon_3}\zeta_3 \end{bmatrix},$$

$$X = \left[A_1\ B_1\ C_1\ D_1\ A_2\ B_2\ A_3\ B_3\ C_3\ D_3\right]^T,$$

and $$Z = \left[\frac{M^2P}{L^2 s_1^2 \varepsilon_1^2}\ 0\ \left(\frac{M^2P}{L^2 s_1^2 \varepsilon_1^2} - \frac{P}{\lambda^2\phi}\right)\ 0\ 0\ -\left(\frac{M^2P}{L^2 s_3^2 \varepsilon_3^2} - \frac{P}{\lambda^2\phi}\right)\ 0\ 0\ \frac{M^2P}{L^2 s_3^2 \varepsilon_3^2}\ 0\right]^T,$$

where $\xi_1 = s_1[-\frac{1}{2} + \frac{L^2(-1+M^2)}{M^4}((-1+M^2)H_1^2 - \eta_1^2) + \frac{s_1^2 L^2(-1+M^2)}{M^4}]$,
$\zeta_1 = \varepsilon_1[-\frac{1}{2} + \frac{L^2(-1+M^2)}{M^4}((-1+M^2)H_1^2 - \eta_1^2) + \frac{\varepsilon_1^2 L^2(-1+M^2)}{M^4}]$,
$\xi_2 = s_1[M^2(-2+M^2) - 2L^2(-1+M^2)((-1+M^2)H_1^2 + s_1^2 - \eta_1^2)]$,
$\zeta_2 = \varepsilon_1[M^2(-2+M^2) - 2L^2(-1+M^2)((-1+M^2)H_1^2 + \varepsilon_1^2 - \eta_1^2)]$,
$\xi_3 = s_3[-\frac{1}{2} + \frac{L^2(-1+M^2)}{M^4}((-1+M^2)H_3^2 - \eta_3^2) + \frac{s_3^2 L^2(-1+M^2)}{M^4}]$,
$\zeta_3 = \varepsilon_3[-\frac{1}{2} + \frac{L^2(-1+M^2)}{M^4}((-1+M^2)H_3^2 - \eta_3^2) + \frac{\varepsilon_3^2 L^2(-1+M^2)}{M^4}]$,
$\xi_4 = s_3[M^2(-2+M^2) - 2L^2(-1+M^2)((-1+M^2)H_3^2 + s_3^2 - \eta_3^2)]$,
$\zeta_4 = \varepsilon_3[M^2(-2+M^2) - 2L^2(-1+M^2)((-1+M^2)H_3^2 + \varepsilon_3^2 - \eta_3^2)]$,
$\Omega = 2M^2\lambda\phi(1-M^2)$.

Using MATHEMATICA, all parameters (*i.e.* $A_1, B_1, C_1, D_1, A_2, B_2, A_3, B_3, C_3, D_3$) have been evaluated uniquely. Due to cumbersome expressions of these parameters, we refrain the values of these parameters from the text of manuscript.

6 Evaluation of flow rate and stresses

6.1 Flow rate

The flow rate through channels ($0 < y < 3$) can be evaluated using the formula:

$$Q = \int_0^1 u_1\,dy + \int_1^2 u_2\,dy + \int_2^3 u_3\,dy. \tag{6.1}$$

Substituting expressions of velocities from Eqs. (4.2) and (4.8) in Eq. (6.1), we are able to find the analytical expression for the volumetric flow rate of Newtonian-micropolar fluid flow. Therefore, the analytical expression of the flow rate will be

$$\begin{aligned} Q = {} & \frac{e^{-2\lambda}\left(e^{\lambda}-1\right)\lambda\left(A_2 e^{3\lambda} + B_2\right) - \frac{P}{\phi}}{\lambda^2} + \frac{A_1(e^{s_1}-1)}{s_1} \\ & + \frac{A_3 e^{2s_3}(e^{s_3}-1)}{s_3} \\ & + \frac{B_1(1-e^{-s_1})}{s_1} + \frac{B_3 e^{-3s_3}(e^{s_3}-1)}{s_3} \\ & + \frac{e^{-\epsilon_1}(e^{\epsilon_1}-1)\epsilon_1\left(C_1 e^{\epsilon_1} + D_1\right) - \frac{M^2P}{L^2 s_1^2}}{\epsilon_1^2} \\ & + \frac{e^{-3\epsilon_3}(e^{\epsilon_3}-1)\epsilon_3\left(C_3 e^{5\epsilon_3} + D_3\right) - \frac{M^2P}{L^2 s_3^2}}{\epsilon_3^2}. \end{aligned} \tag{6.2}$$

6.2 Tangential and couple stresses at the interfaces

6.3 At porous interface y=1:

The non-dimensional form of the tangential stress ($T_{yx(1)}$) and couple stress ($m_{yz(1)}$) at lower interface ($y = 1$) of the porous layers are denoted by $T_{yx}^{(1)}$ and $m_{yz}^{(1)}$, respectively. Mathematically,

$$T_{yx}^{(1)} = \left[\frac{1}{1-M^2}\left(\frac{du_1}{dy}\right) + \left(\frac{M^2}{1-M^2}\right)w_1\right]_{y=1}$$
$$\text{and } m_{yz}^{(1)} = \left[\frac{dw_1}{dy}\right]_{y=1}.$$

Therefore,

$$\begin{aligned} T_{yx}^{(1)} = {} & \frac{1}{2M^2\left(1-M^2\right)} \\ & \big[A_1 e^{s_1} s_1\left(2L^2\left(M^2-1\right)\left(-\eta_1^2 + H_1^2\left(M^2-1\right) + s_1^2\right)\right. \\ & \left. -M^2\left(M^2-2\right)\right) \\ & + B_1 e^{-s_1} s_1\left(M^2\left(M^2-2\right) - 2L^2\left(M^2-1\right)\right. \\ & \left.\left(-\eta_1^2 + H_1^2\left(M^2-1\right) + s_1^2\right)\right) \\ & + e^{-\epsilon_1}\epsilon_1\left(C_1 e^{2\epsilon_1} - D_1\right)\left(2L^2\left(M^2-1\right)\right. \\ & \left.\left(-\eta_1^2 + H_1^2\left(M^2-1\right) + \epsilon_1^2\right) - M^2\left(M^2-2\right)\right)\big]. \end{aligned} \tag{6.3}$$

and

$$\begin{aligned} m_{yz}^{(1)} = {} & \left(\frac{L^2\left(M^2-1\right)\left(H_1^2\left(M^2-1\right) - \eta_1^2\right)}{M^4} - \frac{1}{2}\right) \\ & \left(A_1 e^{s_1} s_1^2 + B_1 e^{-s_1} s_1^2 + e^{-\epsilon_1}\epsilon_1^2\left(C_1 e^{2\epsilon_1} + D_1\right)\right) \\ & + \frac{L^2\left(M^2-1\right)}{M^4} \\ & \left[e^{-s_1-\epsilon_1}\left(A_1 s_1^4 e^{2s_1+\epsilon_1} + B_1 s_1^4 e^{\epsilon_1} + e^{s_1}\epsilon_1^4\left(C_1 e^{2\epsilon_1} + D_1\right)\right)\right]. \end{aligned} \tag{6.4}$$

6.4 At porous interface y=2

The non-dimensional form of the tangential stress ($T_{yx(3)}$) and couple stress ($m_{yz(3)}$) at upper interface ($y = 2$) of the porous layers are denoted by $T_{yx}^{(3)}$ and $m_{yz}^{(3)}$, respectively. Mathematically,

$$T_{yx}^{(3)} = \left[\frac{1}{1-M^2}\left(\frac{du_3}{dy}\right) + \left(\frac{M^2}{1-M^2}\right) w_3\right]_{y=2}$$

$$\text{and} m_{yz}^{(3)} = \left[\frac{dw_3}{dy}\right]_{y=2}.$$

Therefore,

$$\begin{aligned} T_{yx}^{(3)} = {} & \frac{1}{2M^2\left(1-M^2\right)} \\ & [A_3 e^{2s_3} s_3 (2L^2\left(M^2-1\right)\left(-\eta_3^2 + H_3^2\left(M^2-1\right) + s_3^2\right) \\ & - M^2\left(M^2-2\right)) + e^{-2\left(s_3+\epsilon_3\right)}(e^{2s_3}\epsilon_3\left(C_3 e^{4\epsilon_3} - D_3\right) \\ & (2L^2\left(M^2-1\right) \\ & \left(-\eta_3^2 + H_3^2\left(M^2-1\right) + \epsilon_3^2\right) - M^2\left(M^2-2\right)) - B_3 s_3 e^{2\epsilon_3} \\ & (2L^2\left(M^2-1\right)\left(-\eta_3^2 + H_3^2\left(M^2-1\right) + s_3^2\right) - M^2\left(M^2-2\right)))], \end{aligned} \tag{6.5}$$

and

$$\begin{aligned} m_{yz}^{(3)} = {} & \left(\frac{L^2\left(M^2-1\right)\left(H_3^2\left(M^2-1\right) - \eta_3^2\right)}{M^4} - \frac{1}{2}\right) \\ & \left(A_3 s_3^2 e^{s_3 y} + B_3 s_3^2 e^{-s_3 y}\right. \\ & \left. + \epsilon_3^2 e^{-y\epsilon_3}\left(C_3 e^{2y\epsilon_3} + D_3\right)\right) + \frac{L^2\left(M^2-1\right)}{M^4} \\ & \left[e^{-y\left(s_3+\epsilon_3\right)}\left(A_3 s_3^4 e^{y\left(2s_3+\epsilon_3\right)}\right.\right. \\ & \left.\left. + B_3 s_3^4 e^{y\epsilon_3} + \epsilon_3^4 e^{s_3 y}\left(C_3 e^{2y\epsilon_3} + D_3\right)\right)\right]. \end{aligned} \tag{6.6}$$

7 Discussion of flow rate

In this section, we will discuss the variation of the flow rate with respect to permeability parameter (η_2) on micropolar parameter (M), couple stress parameter (L), viscosity ratio (ϕ), Hartmann number (H), permeability parameters (η_1, η_3) and conductivity ratio parameters (Λ_1, Λ_3). Numerical values of flow rate, wall shear stresses and couple stresses at the porous interfaces are mentioned in Tables (1)–(8). To plot graphs of flow rate, pressure gradient ($P = -0.2$) and permeability parameter ($\eta_2 = 0$ to 5) are used.

7.1 Effect of micropolar parameter *M*

Figure 2 shows the effect of micropolar parameter ($M = 0.25,\ 0.5,\ 0.75$) on the flow rate of the fluid flow in the three respective porous regions when couple stress parameter ($L = 0.2$), viscosity ratio parameter ($\phi = 1$), Hartmann number ($H = 1$), permeability parameters ($\eta_1 = 1.2,\ \eta_3 = 1.3$) and conductivity ratio parameters ($\Lambda_1 = 1,\ \Lambda_3 = 2$). As the parameter M grows, the volumetric flow rate decreases in all respective porous channels. The behavior of volumetric flow rate is almost similar for very small values of M. Along the variation of permeability parameter η_2, we observed that the flow rate is rapidly decreasing for very small variation in η_2 and for the large values of η_2, flow rate decreases very slowly. Numerical values of flow rate (Q), shear stresses ($T_{yx(1)}, T_{yx(3)}$) and couple stresses ($m_{yz(1)}, m_{yz(3)}$) at the porous interfaces ($y = 1$ and $y = 2$), (*i.e.* named earlier as $T_{yx}^{(1)}, T_{yx}^{(3)}, m_{yz}^{(1)}, m_{yz}^{(3)}$ in (6.2) and (6.2)), are mentioned in the Table 1.

Table 1 Numerical values of flow rate, shear stresses and couple stresses at porous interfaces for micropolar parameter M when: $P = -0.2,\ L = 0.2,\ \phi = 1,\ H = 1,\ \Lambda_1 = 1,\ \Lambda_3 = 2,\ \eta_1 = 1.2,\ \eta_2 = 0.2,\ \eta_3 = 1.3$

M	Q	$T_{yx}^{(1)}$	$T_{yx}^{(3)}$	$m_{yz}^{(1)}$	$m_{yz}^{(3)}$
0.25	0.213984	0.0452436	0.0528572	9.76996×10^{-15}	1.9984×10^{-14}
0.5	0.190562	0.0473355	0.0577326	1.16504×10^{-14}	9.06289×10^{-14}
0.75	0.133427	0.060169	0.0686321	1.1869×10^{-14}	2.38673×10^{-13}

Table 2 Numerical values of flow rate, wall shear stresses and couple stresses for couple stress parameter L when: $P = -0.2,\ M = 0.25,\ \phi = 1,\ H = 1,\ \Lambda_1 = 1,\ \Lambda_3 = 2,\ \eta_1 = 1.2,\ \eta_2 = 0.2,\ \eta_3 = 1.3$

L	Q	$T_{yx}^{(1)}$	$T_{yx}^{(3)}$	$m_{yz}^{(1)}$	$m_{yz}^{(3)}$
0.02	0.234741	0.0342528	0.0516773	2.32016×10^{-8}	5.14887×10^{-7}
0.2	0.213984	0.0452436	0.0528572	5.77316×10^{-16}	2.22045×10^{-15}
2	0.205468	0.0497552	0.0538453	5.68434×10^{-14}	2.84217×10^{-14}

7.2 Effect of couple parameter *L*

Effect of couple stress parameter ($L = 0.02,\ 0.2,\ 2$) on the flow rate of the fluid flow in the three respective porous regions are reported using Fig. 3 when micropolar parameter ($M = 0.25$), viscosity ratio $\phi = 1$, Hartmann number ($H = 1$), permeability parameter ($\eta_1 = 1.2,\ \eta_3 = 1.3$) and conductivity ratio parameters ($\Lambda_1 = 1,\ \Lambda_3 = 2$). As the couple stress parameter increases, the volumetric flow rate (Q) decreases in all respective porous regions. Behavior of the flow rate is almost similar for large values of this stress parameter. For $\eta_2 > 3$, the behavior of the graph of flow rate is almost same for every value of micropolar parameter. Along the variation of parameter η_2, we found that the flow rate is decreasing rapidly for the small variation of the permeability parameter η_2 and for the large values of this permeability parameter, the flow rate decays smoothly. Numerical values of flow rate, shear stresses and couple stresses at the porous interfaces are given in Table 2.

7.3 Effect of viscosity ratio parameter ϕ

Figure 4 represents the effect of viscosity parameter (ϕ) on the flow rate of the fluid flow in the three respective porous regions when micropolar parameter ($M = 0.25$), couple stress parameter ($L = 2$), Hartmann number ($H = 1.1$), permeability parameter ($\eta_1 = 1.2,\ \eta_3 = 1.3$) and conductivity ratio parameters ($\Lambda_1 = 1, \Lambda_3 = 2$) are substituted. As the viscosity parameter (ϕ) increases, the volumetric flow rate decreases in all respective porous regions. Along the variation of parameter (η_2), we observed that the flow rate is decreasing rapidly for the small variation of permeability parameter and for the large values of this ratio parameter, the flow rate is decreasing slowly. Numerical values of flow rate, wall shear stresses and couple stresses at the porous interfaces are given in Table 3.

7.4 Effect of Hartmann number *H*

Effect of magnetic parameter (H) on the flow rate is described in the three respective fluid flow regions when micropolar parameter ($M = 0.25$), couple stress parameter ($L = 2$), viscosity ratio parameter ($\phi = 1$), conductivity ratio parameter ($\Lambda_1 = 1, \Lambda_3 = 2$), and permeability parameter ($\eta_1 = 1.2,\ \eta_3 = 1.3$) (Fig. 5). As the Hartmann number (H) increases, the volumetric flow rate decreases in all regions whenever permeability parameter $\eta_2 < 2.5$. Now,

Table 3 Numerical values of flow rate, wall shear stresses and couple stresses for viscosity ratio parameter ϕ when: $P = -0.2,\ M = 0.25,\ L = 2,\ H = 1,\ \Lambda_1 = 1,\ \Lambda_3 = 2,\ \eta_1 = 1.2,\ \eta_2 = 0.2,\ \eta_3 = 1.3$

ϕ	Q	$T_{yx}^{(1)}$	$T_{yx}^{(3)}$	$m_{yz}^{(1)}$	$m_{yz}^{(3)}$
0.5	0.210468	0.0480615	0.0510098	5.68434×10^{-14}	2.84217×10^{-14}
1	0.205468	0.0497552	0.0538453	5.68434×10^{-14}	0
1.5	0.203164	0.0498231	0.0546027	0	5.68434×10^{-14}

Table 4 Numerical values of flow rate, wall shear stresses and couple stresses for Hartmann number H when: $P = -0.2,\ M = 0.25,\ L = 2,\ \phi = 1,\ \Lambda_1 = 1,\ \Lambda_3 = 2,\ \eta_1 = 1.2,\ \eta_2 = 0.2,\ \eta_3 = 1.3$

H	Q	$T_{yx}^{(1)}$	$T_{yx}^{(3)}$	$m_{yz}^{(1)}$	$m_{yz}^{(3)}$
0.01	0.0266632	0.0944174	0.100186	3.55271×10^{-15}	4.61853×10^{-14}
0.5	0.244019	0.0808337	0.084528	2.84217×10^{-14}	2.84217×10^{-14}
1	0.205468	0.0497552	0.0538453	5.68434×10^{-14}	0

Table 5 Numerical values of flow rate, wall shear stresses and couple stresses for Λ_1 when: $P = -0.2,\ M = 0.25,\ L = 0.2,\ \phi = 1,\ H = 1,\ \Lambda_3 = 2,\ \eta_1 = 1.2,\ \eta_2 = 0.2,\ \eta_3 = 1.3$

Λ_1	Q	$T_{yx}^{(1)}$	$T_{yx}^{(3)}$	$m_{yz}^{(1)}$	$m_{yz}^{(3)}$
0.75	0.218176	0.043378	0.0536682	2.93099×10^{-14}	1.26656×10^{-14}
1.5	0.210477	0.0465373	0.0522948	3.55271×10^{-15}	0
5	0.206657	0.0473776	0.0.0519295	1.77636×10^{-15}	6.66134×10^{-16}

Table 6 Numerical values of flow rate, wall shear stresses and couple stresses for Λ_3 when: $P = -0.2,\ M = 0.25,\ L = 2,\ \phi = 1,\ H = 1,\ \Lambda_1 = 1,\ \eta_1 = 1.2,\ \eta_2 = 0.2,\ \eta_3 = 1.3$

Λ_3	Q	$T_{yx}^{(1)}$	$T_{yx}^{(3)}$	$m_{yz}^{(1)}$	$m_{yz}^{(3)}$
0.6	0.213768	0.0500216	0.0532525	5.68434×10^{-14}	3.41061×10^{-13}
1	0.20787	0.0493608	0.0547232	0	5.68434×10^{-14}
3	0.205104	0.500975	0.0530837	5.68434×10^{-14}	2.84217×10^{-14}

Table 7 Numerical values of flow rate, wall shear stresses and couple stresses for permeability parameter η_1 when: $P = -0.2,\ M = 0.25,\ L = 0.2,\ \phi = 1,\ H = 1,\ \Lambda_1 = 1,\ \Lambda_3 = 2,\ \eta_2 = 0.2,\ \eta_3 = 1.3$

η_1	Q	$T_{yx}^{(1)}$	$T_{yx}^{(3)}$	$m_{yz}^{(1)}$	$m_{yz}^{(3)}$
1	0.22536	0.0372195	0.0563454	7.9492×10^{-14}	3.37508×10^{-14}
1.5	0.197595	0.0568309	0.0478201	6.21725×10^{-15}	9.99201×10^{-15}
2	0.17424	0.0734248	0.0406065	2.66454×10^{-15}	4.44089×10^{-15}

Table 8 Numerical values of flow rate, wall shear stresses and couple stresses for permeability parameter η_3 when: $P = -0.2,\ M = 0.25,\ L = 0.2,\ \phi = 1,\ H = 1,\ \Lambda_1 = 1,\ \Lambda_3 = 2,\ \eta_1 = 1.2,\ \eta_2 = 0.2$

η_3	Q	$T_{yx}^{(1)}$	$T_{yx}^{(3)}$	$m_{yz}^{(1)}$	$m_{yz}^{(3)}$
0.75	0.249411	0.0536507	0.0333265	1.77636×10^{-15}	1.63425×10^{-13}
1	0.229411	0.0499282	0.0419743	1.33227×10^{-15}	4.57412×10^{-14}
1.5	0.20403	0.042212	0.0598999	1.77636×10^{-15}	2.22045×10^{-16}

for $\eta_2 > 2.5$, the flow rate is increasing with the increment in the Hartmann number H. Along with the small variation of this ratio parameter (η_2), we see that the flow rate is decreasing rapidly and for $\eta_2 > 2.5$, flow rate is almost coincided. Numerical values of flow rate (Q), wall shear stresses ($T_{yx}^{(1)}, T_{yx}^{(3)}$) and couple stresses ($m_{yz}^{(1)}, m_{yz}^{(3)}$) are mentioned in Table 4.

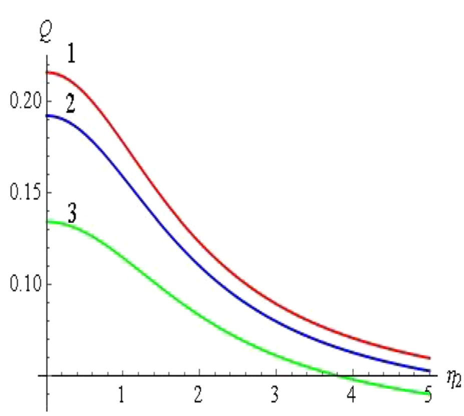

Fig. 2 Variation of the flow rate: (1) $M = 0.25$, (2) $M = 0.5$, (3) $M = 0.75$

7.5 Effect of conductivity ratio parameter Λ_1

Effect of conductivity ratio parameter (Λ_1) on the flow rate in the three respective porous regions (Fig. 6) when micropolar parameter ($M = 0.25$), couple stress parameter ($L = 0.2$), viscosity ratio parameter ($\phi = 1$), Hartmann number ($H = 1$), conductivity ratio parameter ($\Lambda_3 = 2$), and permeability parameters ($\eta_1 = 1.2,\ \eta_3 = 1.3$) is discussed. The flow rate decreases in all porous regions with the increment in the values of the parameter (Λ_1). For the large value of conductivity ratio parameter Λ_1, the behavior of flow rate

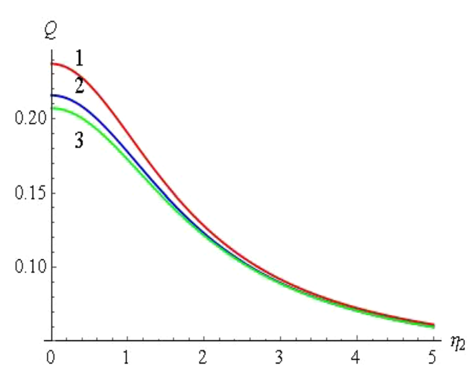

Fig. 3 Variation of the flow rate: (1) $L = 0.02$, (2) $L = 0.2$, (3) $L = 2$

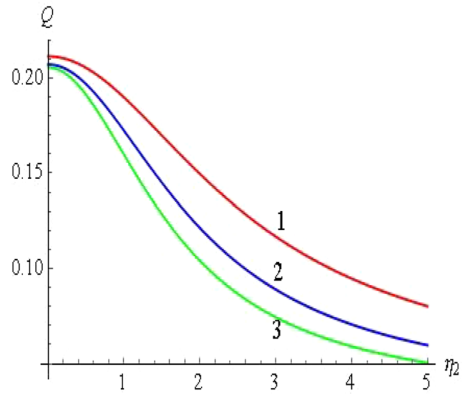

Fig. 4 Variation of the flow rate: (1) $\phi = 0.5$, (2) $\phi = 1$, (3) $\phi = 1.5$

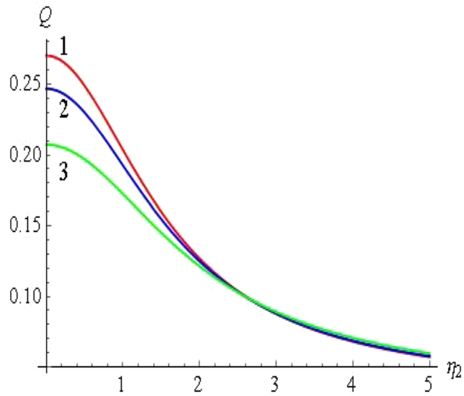

Fig. 5 Variation of the flow rate: (1) $H = 0.01$, (2) $H = 0.5$, (3) $H = 1$

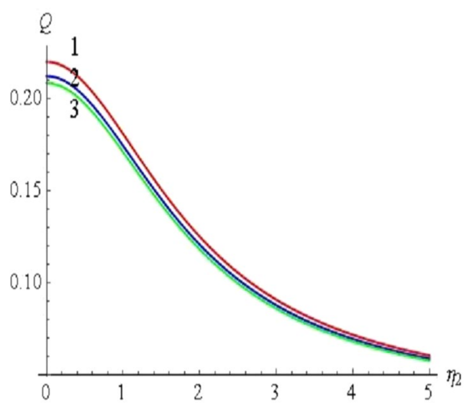

Fig. 6 Variation of the flow rate: (1) $\Lambda_1 = 0.75$, (2) $\Lambda_1 = 1.5$, (3) $\Lambda_1 = 5$

is similar. In addition, the flow rate is decaying rapidly whenever $\eta_2 < 3$ and for $\eta_2 > 3$, the similar variations in the flow rate are found for every values of Λ_1. For the porous interfaces ($y = 1$ and $y = 2$), numerical values of flow rate (Q), wall shear stresses ($T_{yx(1)}, T_{yx(3)}$) and couple stresses ($m_{yz(1)}, m_{yz(3)}$) are written in Table 5.

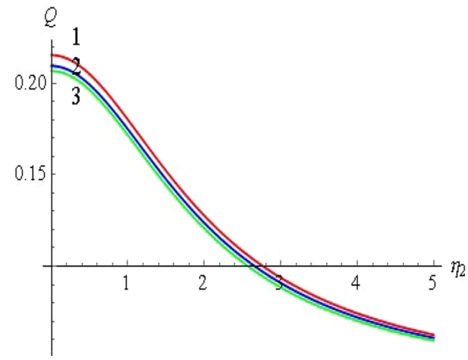

Fig. 7 Variation of the flow rate: (1) $\Lambda_3 = 0.6$, (2) $\Lambda_3 = 1$, (3) $\Lambda_3 = 3$

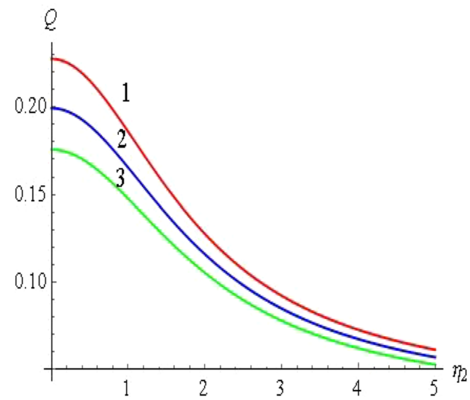

Fig. 8 Variation of the flow rate: (1) $\eta_1 = 1$, (2) $\eta_1 = 1.5$, (3) $\eta_1 = 2$

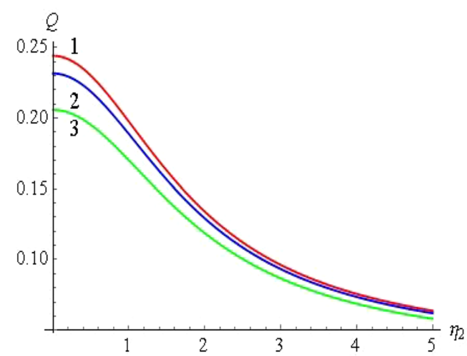

Fig. 9 Variation of the flow rate: (1) $\eta_3 = 0.75$, (2) $\eta_3 = 1$, (3) $\eta_3 = 1.5$

7.6 Effect of conductivity ratio parameter Λ_3

Effect of conductivity ratio parameter (Λ_3) on the flow rate in the three respective porous regions (Fig. 7) when micropolar parameter ($M = 0.25$), couple stress parameter ($L = 2$), viscosity ratio parameter ($\phi = 1$), Hartmann number ($H = 1$), conductivity ratio parameter ($\Lambda_1 = 1$), and permeability parameters ($\eta_1 = 1.2,\ \eta_3 = 1.3$) is discussed. For all value of conductivity ratio parameter Λ_3, the flow rate is almost same for all the values of η_2. The volumetric flow rate decreases in respective porous regions as the values of the parameter (Λ_1) increases. In addition, the flow rate is decaying rapidly whenever $\eta_2 < 4$ and for $\eta_2 > 4$, decreases very slowly for every values of Λ_3. At the porous interfaces ($y = 1$ and $y = 2$), numerical values of flow rate (Q), wall shear stresses ($T_{yx(1)}, T_{yx(3)}$) and couple stresses ($m_{yz(1)}, m_{yz(3)}$) are given in Table 6.

7.7 Effect of permeability parameter η_1

Effects of permeability parameter (η_1) on the flow rate in the three respective porous regions are discussed when $M = 0.25,\ L = 0.2,\ \phi = 1,\ H = 1,\ \Lambda_1 = 1,\ \Lambda_3 = 2,\ \eta_3 = 1.3$ (Fig. 8). Volumetric flow rate decreases in all respective porous regions whenever the parameter (η_1) increases. In addition, we observed that for a fixed value of η_1, the flow rate is decreasing rapidly for the small variation of the permeability parameter (η_2) and for the large values of η_2, the flow rate decreases slowly. In addition, for the large variation in η_2, flow rate is converging therefore, streamlines become very close to each other. Numerical values of flow rate (Q), wall shear stresses ($T^{(1)}_{yx}, T^{(3)}_{yx}$) and couple stresses ($m^{(1)}_{yz}, m^{(3)}_{yz}$) are mentioned in Table 7.

7.8 Effect of permeability parameter η_3

Effects of permeability parameter (η_3) on the flow rate of the fluid flow in the three respective porous regions are explained by Fig. 9 when values of micropolar parameter, couple stress parameter, viscosity ratio parameter, Hartmann number, conductivity ratio parameters, and permeability parameter are taken as $M = 0.25,\ L = 0.2,\ \phi = 1,\ H = 1,\ \Lambda_1 = 1,\ \Lambda_3 = 2,\ \eta_1 = 1.2$, respectively. As the permeability parameter η_3 increases, the volumetric flow rate decreases in all respective porous regions. Graphs of flow rate are looking similar for every values of η_2 whenever, the parameter η_3 decreases. Flow rate is decaying rapidly for small variation of permeability parameter η_2 and the streamlines passing through a cross-section coincide to each other for the large values of η_2. Numerical values of flow rate, wall shear stresses and couple stresses at the porous interfaces are mentioned in Table 8.

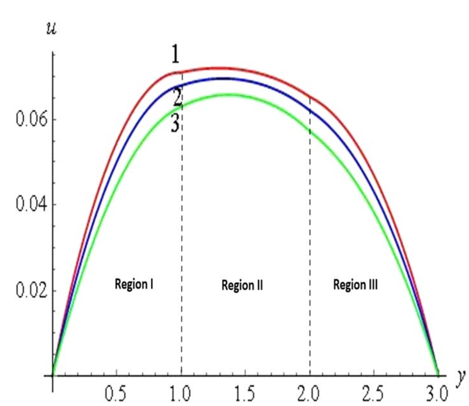

Fig. 10 Variation of the fluid velocity: (1) $M = 0.4$, (2) $M = 0.5$, (3) $M = 0.6$

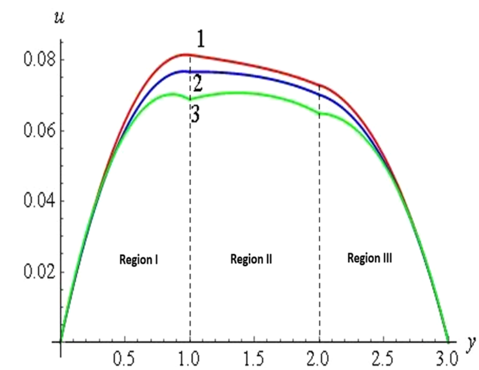

Fig. 11 Variation of the fluid velocity: (1) $L = 0.01$, (2) $L = 0.1$, (3) $L = 1$

8 Discussion of the fluid velocity

In this section, we will discuss the graphical behavior of the fluid velocity along with the variation of width of channel y in which pressure gradient $P = -0.2$ is kept fixed for the following parameters: (i) effect of micropolar parameter (M), (ii) effect of couple stress parameter (L), (iii) effect of viscosity ratio parameter (ϕ), (iv) effect of Hartmann number (H), (v) effect of conductivity ratio parameter (Λ_1), (vi) effect of conductivity ratio parameter (Λ_3), (vii) effect of permeability parameter (η_1), (viii) effect of permeability parameter (η_2), and (ix) effect of permeability parameter (η_3).

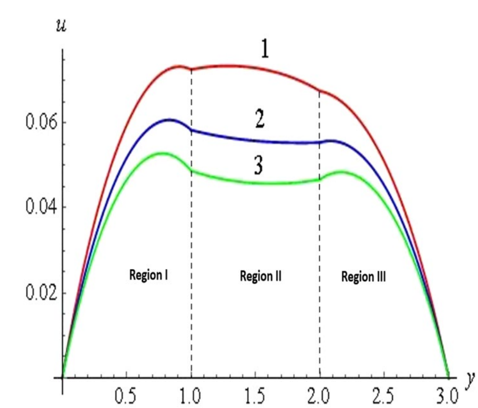

Fig. 12 Variation of the fluid velocity: (1) $\phi = 1$, (2) $\phi = 2$, (3) $\phi = 3$

8.1 Effect of micropolar parameter *M*

Effects of micropolar parameter ($M = 0.4,\ 0.5,\ 0.6$) on the fluid velocity in the three respective porous regions are discussed when couple stress parameter ($L = 0.2$), viscosity ratio parameter ($\phi = 1$), Hartmann number ($H = 1$), conductivity ratio parameters ($\Lambda_1 = 1,\ \Lambda_3 = 2$), and permeability parameters: $\eta_1 = 1.1,\ \eta_2 = 1.2,\ \eta_3 = 1.3$ (Fig. 10). The velocity of fluid flow through channels decreases whenever the parameter M increases and streamlines are parabolic. In addition, we observed that the velocity profile on the width of the channel y varies up to a maximum values whenever $y < 1$, almost constant for $1 < y < 2$ and decreases smoothly for $y > 2$. Near the walls (both lower and upper), velocity vanishes due to presence of no slip conditions at walls (*i.e.* $y = 0$ and $y = 3$).

8.2 Effect of couple stress parameter *L*

Effects of couple stress parameter ($L = 0.01,\ 0.1,\ 1$) on the fluid velocity in the all porous regions when micropolar parameter ($M = 0.25$), viscosity ratio parameter ($\phi = 1$), Hartmann number ($H = 1$), conductivity ratio parameters ($\Lambda_1 = 1,\ \Lambda_3 = 2$), and permeability parameters ($\eta_1 = 1.1,\ \eta_2 = 1.2,\ \eta_3 = 1.3$) are discussed (Fig. 11). Velocity of fluid flow through channels decreases whenever the couple stress parameter L increases and the streamlines are parabolic. In addition, we observed that the velocity profile on the width of the channel y varies up to a maximum value whenever $y < 1$, varies constantly for $1 < y < 2$ and decays smoothly for $y > 2$.

8.3 Effect of viscosity ratio parameter *ϕ*

Figure 12 represents the effect of viscosity ratio parameter ($\phi = 1,\ 2,\ 3$) on the fluid velocity in the three respective porous regions when micropolar parameter ($M = 0.25$), couple stress parameter ($L = 0.2$), Hartmann number ($H = 1$), conductivity ratio parameters ($\Lambda_1 = 1,\ \Lambda_3 = 2$), and permeability parameters ($\eta_1 = 1.1,\ \eta_2 = 1.2,\ \eta_3 = 1.3$) are used. Velocity of fluid flow through porous channels decreases as parameter ϕ increases. In addition, it is seen that the velocity profile on the width of the channel y varies up to a maximum value whenever $y < 1$, varies constantly for $1 < y < 2$ and decays smoothly for $y > 2$. Streamlines are fluctuating in the middle porous region which is filled by the Newtonian fluid.

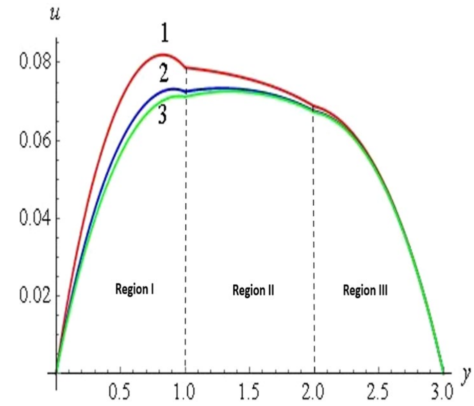

Fig. 14 Variation of the fluid velocity: (1) $\Lambda_1 = 0.5$, (2) $\Lambda_1 = 1$, (3) $\Lambda_1 = 1.5$

8.4 Effect of Hartmann number *H*

Effects of the Hartmann number ($H = 0.75,\ 1,\ 1.25$) on the fluid velocity in three respective porous regions are explained when micropolar parameter ($M = 0.25$), couple stress parameter ($L = 0.2$), viscosity ratio ($\phi = 1$), conductivity ratio parameters ($\Lambda_1 = 1,\ \Lambda_3 = 2$), and permeability parameters: $\eta_1 = 1.1,\ \eta_2 = 1.2,\ \eta_3 = 1.3$ (Fig. 13). When the values of width of channel $y < 1$, the velocity of fluid flow through porous channels increases as parameter H increases and for middle channel ($1 < y < 2$), it decreases as H increases. For $y > 2$,

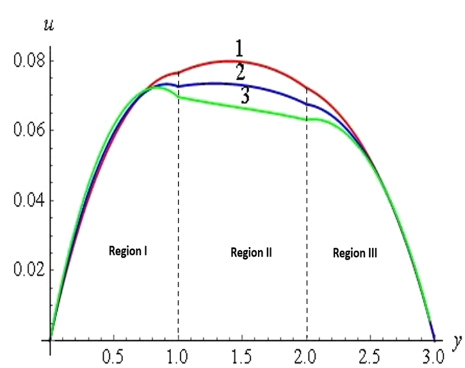

Fig. 13 Variation of the fluid velocity: (1) $H = 0.75$, (2) $H = 1$, (3) $H = 1.25$

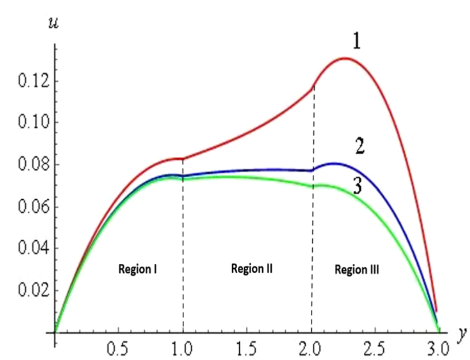

Fig. 15 Variation of the fluid velocity: (1) $\Lambda_3 = 0.2$, (2) $\Lambda_3 = 0.4$, (3) $\Lambda_3 = 0.8$

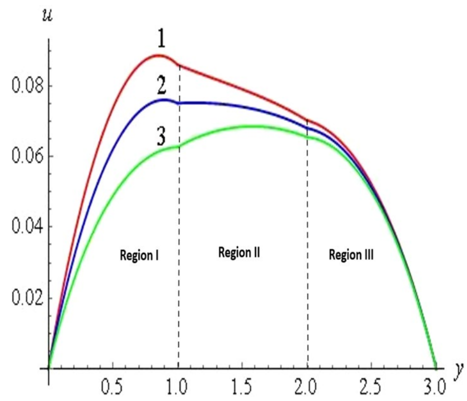

Fig. 16 Variation of the fluid velocity: $(1)\eta_1 = 0.5, (2)\eta_1 = 1, (3)\eta_1 = 1.5$

velocity profiles are found almost same for all values of H. Streamlines are parabolic and the velocity profile for width of the channel y varies whenever $y < 1$. In addition, the velocity decays slowly within the region $(1 < y < 2)$ and rapidly for $y > 2$.

8.5 Effect of conductivity ratio parameter Λ_1

Effects of conductivity ratio parameter $(\Lambda_1 = 0.5, 1, 1.5)$ on the fluid velocity in the three respective porous regions are discussed using Fig. 14 when micropolar parameter $(M = 0.25)$, couple stress parameter $(L = 0.2)$, viscosity ratio $(\phi = 1)$, Hartmann number $(H = 1)$, conductivity ratio parameter $(\Lambda_3 = 2)$, and permeability parameters $(\eta_1 = 1.1,\ \eta_2 = 1.2,\ \eta_3 = 1.3)$ are used. The velocity of fluid flow through porous channels decreases as parameter Λ_1 increases in all fluid regions. For large values of y, velocity profiles are same for all values of Λ_1. The nature of streamlines are looking as parabolic.

8.6 Effect of conductivity ratio parameter Λ_3

Effects of conductivity ratio parameter $(\Lambda_3 = 0.2, 0.4, 0.8)$ on the fluid velocity in the three respective porous regions are described (Fig. 15) when micropolar parameter $(M = 0.25)$, couple stress parameter $(L = 0.2)$, viscosity ratio $(\phi = 1)$, Hartmann number $(H = 1)$, conductivity ratio parameter $(\Lambda_1 = 1)$, and permeability parameters $(\eta_1 = 1.1,\ \eta_2 = 1.2,\ \eta_3 = 1.3$. Velocity of fluid flow through porous channels decreases as parameter Λ_3 increases in all fluid regions. For very small values of y, velocity profiles are same for all values of Λ_3 and for large values of y, different graphs are obtained. In addition, in fluid velocity, more fluctuations can be seen in the region $(2 < y < 3)$ for small values of Λ_3.

8.7 Effect of permeability parameter η_1

Figure 16 shows the effect of permeability parameter $(\eta_1 = 0.5, 1, 1.5)$ on the fluid velocity in the three respective porous regions when value of micropolar parameter $(M = 0.25)$, couple stress parameter $(L = 0.2)$, viscosity ratio $(\phi = 1)$, Hartmann number $(H = 1)$, conductivity ratio parameters $(\Lambda_1 = 1,\ \Lambda_3 = 2)$, and permeability parameters $(\eta_2 = 1.2,\ \eta_3 = 1.3)$ are taken. As the permeability parameter η_1 increases, fluid velocity through porous channels decreases. For $y > 2.5$, similar velocity profiles are obtained for all values of η_1. Behavior of streamlines are of parabolic. For the small values of y, different graphs are obtained.

8.8 Effect of permeability parameter η_2

Effects of permeability parameter $(\eta_2 = 0.5, 1, 1.5)$ on the fluid velocity (Fig. 17) in the three respective porous regions when micropolar parameter $(M = 0.25)$, couple stress parameter $(L = 0.2)$, viscosity ratio $(\phi = 1)$, Hartmann number

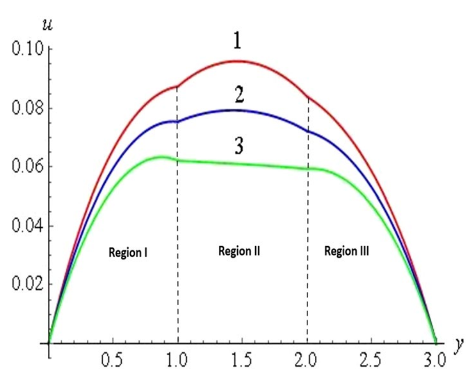

Fig. 17 Variation of the fluid velocity: (1) $\eta_2 = 0.5$, (2) $\eta_2 = 1$, (3) $\eta_2 = 1.5$

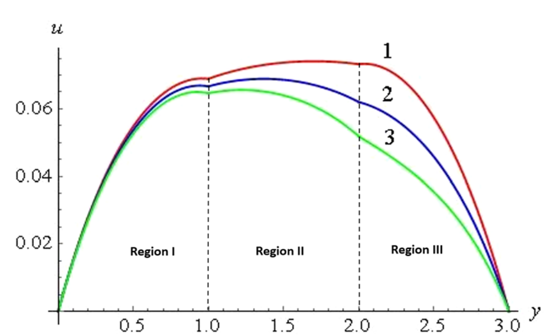

Fig. 18 Variation of the fluid velocity: (1) $\eta_3 = 1$, (2) $\eta_3 = 1.5$, (3) $\eta_3 = 2$

($H = 1$), conductivity ratio parameters ($\Lambda_1 = 1,\ \Lambda_3 = 2$), and permeability parameters ($\eta_1 = 1.2,\ \eta_3 = 1.3$) are discussed. As the permeability parameter η_2 increases, the fluid velocity through porous channels decreases. For the regions $y < 0.5$ and $y > 2.5$, velocity profiles are similar for all values of η_2. Behavior of streamlines are of parabolic. In addition, for the region $0.5 < y < 2.5$, different graphs are obtained for every value of η_2. In addition, for a fixed value of η_2, we found that velocity increases up to a maximum value when $y = 1.5$.

8.9 Effect of permeability parameter η_3

Effect of permeability parameter ($\eta_3 = 1, 1.5, 2$) on the fluid velocity in the three respective porous regions are described with the help of Fig. 18 when micropolar parameter ($M = 0.25$), couple stress parameter ($L = 0.2$), viscosity ratio ($\phi = 1$), Hartmann number ($H = 1$), conductivity ratio parameters ($\Lambda_1 = 1,\ \Lambda_3 = 2$), and permeability parameters ($\eta_1 = 1.3,\ \eta_2 = 1.2$) are substituted. As the permeability parameter η_3 increases, the fluid velocity through porous channels decreases. For the region $0 < y < 1$, almost similar variations are obtained and variations of streamlines for region $1 < y < 3$ are different.

9 Conclusion

In this research work, we have investigated the micropolar–Newtonian flow through composite porous channels in the presence of magnetic field. The volumetric flow rate and fluid velocity are plotted for different values of various parameters and these parameters are such as micropolar parameter (M), couple stress parameter (L), viscosity ratio parameter (ϕ), Hartmann number (H), conductivity ratio parameters ($\Lambda_1,\ \Lambda_3$), and permeability parameters ($\eta_1,\ \eta_2,\ \eta_3$). Numerical values of flow rate, tangential stresses and couple stresses at both porous interfaces (*i.e.* $y = 1$ and $y = 2$) are calculated by MATHEMATICA and listed in tables. Investigating the effect of these parameters, following conclusions are made:

- The fluid flow rate through the cross-section of channels, decreases in each case when either M increases or L increases or ϕ increases or H increases or Λ_1 increases or Λ_3 increases or η_1 increases or η_2 increases or η_3 increases.
- The fluid velocity passing through respective porous channels, decreases in each case when either M increases or L increases or ϕ increases or H increases or Λ_1 increases or Λ_3 increases or η_1 increases or η_2 increases or η_3 increases. The velocity profile is looking approximately parabolic in each case.
- The obtained results can be utilized for investigating the industrial problems associated with the filtration and purification of contaminated groundwater, oil recovery process through non-homogeneous reservoir, circulation of blood flow through veins of human body, etc. These results can also be used for solving the problem of cooling and heating process of refrigerator (air conditioned), problem of sedimentation, etc.

Acknowledgements Deepak Kumar Maurya acknowledges with thanks to the organizer of international web conference on "Membrane Process Modeling" in the celebration of 60^{th} anniversary of the Prof. A.N. Filippov for giving a chance to present the core idea of the present research work (Deo and Maurya 2020). The authors are grateful to reviewers for their valuable suggestions which have served to improve the manuscript presentation.

Declarations

Conflict of interest The authors of the manuscript declare that they have no conflict of interest.

References

Asia Y, Kashif A, Muhammad A (2016) MHD unsteady flow and heat transfer of micropolar fluid through porous channel with expanding or contracting walls. J Appl Fluid Mech 9:1807–1817

Brinkman HC (1947) A calculation of viscous force exerted by a flowing fluid on a dense swarm of particles. Appl Sci Res A1:27–34

Deo S, Maurya DK (2019) Generalized stream function solution of the Brinkman equation in the cylindrical polar coordinates. Spec Top Rev Porous Med 10:421–428

Deo S, Maurya DK, Filippov AN (2020) Influence of magnetic field on micropolar fluid flow in a cylindrical tube enclosing an impermeable core coated with porous layer. Colloid J 82:649–660

Deo S, Maurya DK, Filippov AN (2021) Effect of magnetic field on hydrodynamic permeability of biporous membrane relative to micropolar liquid flow. Colloid J 83:662–675

Deo S, Maurya DK (2020) MHD effects on micropolar-Newtonian fluid flow through composite porous channel. MPM-Filippov-60-Conference, pp 48–49

Eringen AC (1966) Theory of micropolar fluids. J Math Mech 16:1–18

Jaiswal S, Yadav PK (2020) Flow of micropolar-Newtonian fluids through the composite porous layered channel with movable interfaces. Arab. J Sci Engng 45:921–934

Krishna MV, Reddy MG, Chamkha AJ (2019) Heat and mass transfer on MHD free convective flow over an infinite nonconducting vertical flat porous plate. Int J Fluid Mech Res. 46:1–25

Krishna MV, Sravanthi CS, Gorla RS (2020) Hall and ion slip effects on MHD rotating flow of ciliary propulsion of microscopic organism through porous media. Int Commun Heat Mass Transf 112:104500

Krishna MV, Swarnalathamma BV, Chamkha AJ (2019) Investigations of Soret, Joule and Hall effects on MHD rotating mixed convective flow past an infinite vertical porous plate. J Ocean Engng Sci 4:263–275

Krishna MV, Chamkha AJ (2022) Thermo-diffusion, chemical reaction, Hall and ion slip effects on MHD rotating flow of micro-polar

fluid past an infinite vertical porous surface. Int J Ambient Energy https://doi.org/10.1080/01430750.2021.1946146
Lok YY, Ishak A, Pop I (2018) Oblique stagnation slip flow of a micropolar fluid towards a stretching/shrinking surface: A stability analysis. Chin J Phys 56:3062–3072
Lukaszewicz G (1999) Micropolar Fluids: Theory and Applications. Springer, New York
Maurya DK, Deo S (2020) Stream function solution of the Brinkman equation in parabolic cylindrical coordinates. Int J Appl Comput Math 6:167
Maurya DK, Deo S (2022) Effect of magnetic field on Newtonian fluid sandwiched between non-Newtonian fluids through porous cylindrical shells. Spec Top Rev Porous Media 13:75–92
Maurya DK, Deo S, Khanukaeva DY (2021) Analysis of Stokes flow of micropolar fluid through a porous cylinder. Math Meth Appl Sci 44:6647–6665
Murthy JVR, Sai KS, Bahali NK (2011) Steady flow of micropolar fluid in a rectangular channel under transverse magnetic field with suction. AIP Adv 1:032123. https://doi.org/10.1063/1.3624837
Nield DA, Bejan A (2006) Convection in Porous Media. Springer, New York
Nowacki W (1970) Theory of Micropolar Elasticity. Springer, New York
Sherief HH, Faltas MS, Ashmawy EA, Hameid AMA (2014) Parallel and perpendicular flows of a micropolar fluid between slip cylinder and coaxial fictitious cylindrical shell in cell models. Eur Phys J Plus 129:217
Srinivasacharya D, Murthy JVR, Venugopalam D (2001) Unsteady Stokes flow of micropolar fluid between two parallel porous plates. Int J Engng Sci 39:1557–1563
Srinivasacharya D, Shiferaw M (2009) Hydromagnetic effects on the flow of a micropolar fluid in a diverging channel. Z Angew Math Mech 89:123–131
Srivastava BG, Deo S (2013) Effect of magnetic field on the viscous fluid flow in a channel filled with porous medium of variable permeability. Appl Math Comput 219:8959–8964
Stokes VK (1984) Theories of Fluids with Microstructure. Springer, New York
Umavathi JC, Chamkha AJ, Sridhar KSR (2010) Generalized plain Couette flow and heat transfer in a composite channel. Trans Porous Med 85:157–169
Yadav PK, Jaiswal S, Asim T, Mishra R (2018) Influence of a magnetic field on the flow of a micropolar fluid sandwiched between two Newtonian fluid layers through a porous medium. Eur Phys J Plus 133:247
Yadav PK, Jaiswal S, Sharma BD (2018) Mathematical model of micropolar fluid in two-phase immiscible fluid flow through porous channel. Appl Math Mech 39:993–1006
Yadav PK, Tiwari A, Deo S, Yadav MK, Filippov A, Vasin S, Sherysheva E (2013) Hydrodynamic permeability of biporous membrane. Colloid J 75:473–482